Available online at www.sciencedirect.com
SCIENCE DIRECT®
Journal of Organometallic Chemistry 690 (2005) 2880–2887
Journal of Organometallic Chemistry
www.elsevier.com/locate/jorganchem

Reactivity of C_6F_5S-$P(C_6H_5)_2$ with $[M_3(CO)_{12}]$ (M = Fe, Ru, Os). The X-ray crystal structures of $[Fe_2(\mu\text{-}SC_6F_5)(\mu\text{-}PPh_2)(CO)_6]$, $[Ru_4(\mu_3\text{-}SPPh_2)_2(\mu\text{-}SC_6F_5)_2(\mu\text{-}PPh_2)_2(SC_6F_5)_2(CO)_6]$ and $[Os_3(\eta^1\text{-}Ph_2P\text{-}SC_6F_5)(CO)_{11}]$

Oscar Baldovino-Pantaleón, Gustavo Ríos-Moreno, Ruben A. Toscano, David Morales-Morales *

Instituto de Química, Universidad Nacional Autónoma de México, Cd. Universitaria, Circuito Exterior, Coyoacán, 04510 México city, México

Received 30 November 2004; revised 9 February 2005; accepted 10 February 2005
Available online 25 April 2005

Abstract

The thiophosphinite C_6F_5S-$P(C_6H_5)_2$ (**1**) was synthesized and its reactivity explored with transition metal clusters of group 8. The reaction of **1** with $[M_3(CO)_{12}]$ (M = Fe, Ru, Os) afforded the complexes $[Fe_2(\mu\text{-}SC_6F_5)(\mu\text{-}PPh_2)(CO)_6]$ (**2**), $[Ru_4(\mu_3\text{-}SPPh_2)_2(\mu\text{-}SC_6F_5)_2(\mu\text{-}PPh_2)_2(SC_6F_5)_2(CO)_6]$ (**3**) and $[Os_3(\eta^1\text{-}Ph_2P\text{-}SC_6F_5)(CO)_{11}]$ (**4**) in good yields. Complex **2** was the result of the P–S bond activation, while complex **3** resulted from the activation of P–S and C–S bonds. Simple ligand substitution occurs when C_6F_5S-$P(C_6H_5)_2$ (**1**) is reacted with $Os_3(CO)_{12}$.

Keywords: P–S ligand; Thiophosphinite; Cluster chemistry; Fluorinated thiolate complexes; Crystal structures

1. Introduction

Transition metal carbonyl clusters containing chalcogenides have important chemical and structural significance, since they can be regarded as discrete molecular models of extended inorganic solids [1]. These compounds have also been employed as homogeneous models to better understand the fundamental steps of the catalytic HDS (hydrodesulfurization) process [2] in which sulfur is removed from thiols and other organosulfur compounds in fossil fuels [3]. On the other hand, transition metal clusters containing phosphido ligands have received considerable attention in recent years due to the importance that these compounds may have as homogeneous catalyst and for precursors for semiconductors with low band gaps [4]. Therefore, following our interest in the reactivity of fluorinated thiolates on the one hand and the design and synthesis of robust complexes for application as catalysts in industrially relevant transformations [5], we have synthesized the thiophosphinite C_6F_5S-$P(C_6H_5)_2$ (**1**). Our aim was to have a convenient source of thiolate and secondary phosphines and to explore its reactivity with a series of transition metals clusters of group 8 $[M_3(CO)_{12}]$ (M = Fe, Ru, Os). The results are reported herein.

2. Experimental

2.1. Materials and methods

Unless stated otherwise, all reactions were carried out under an atmosphere of dinitrogen using

* Corresponding author. Tel.: +525556224514; fax: +525556162217.
E-mail address: damor@servidor.unam.mx (D. Morales-Morales).

0022-328X/$ - see front matter © 2005 Elsevier B.V. All rights reserved.
doi:10.1016/j.jorganchem.2005.02.046

conventional Schlenk glassware. Solvents were dried using standard procedures and distilled under dinitrogen immediately prior to use. The IR spectra were recorded on a Nicolet-Magna 750 FT-IR spectrometer as nujol mulls. The ^{1}H NMR (300 MHz) spectra were recorded on a JEOL GX300 spectrometer. Chemical shifts are reported in ppm down field of TMS using the residual solvent ($CDCl_3$, $\delta = 7.27$) as an internal standard. $^{31}P\{^1H\}$NMR (121 MHz) and $^{19}F\{^1H\}$spectra were recorded with complete proton decoupling and are reported in ppm using 85% H_3PO_4 and C_6F_6 as external standards, respectively. Elemental analyses were determined on a Perkin–Elmer 240. Positive-ion FAB mass spectra were recorded on a JEOL JMS-SX102A mass spectrometer operated at an accelerating voltage of 10 kV. Samples were desorbed from a nitrobenzyl alcohol (NOBA) matrix using 3 keV xenon atoms. Mass measurements in FAB are performed at a resolution of 3000 using magnetic field scans and the matrix ions as the reference material or, alternatively, by electric field scans with the sample peak bracketed by two (polyethylene glycol or cesium iodide) reference ions. Melting points were determined in a MEL-TEMP capillary melting point apparatus and are reported without correction. GC–MS analyses were performed on a Agilent 6890N GC with a 30.0 m DB-5 capillary column coupled to an Agilent 5973 Inert Mass Selective detector.

The HSC_6F_5, PPh_2Cl were obtained commercially from Aldrich Chem. Co. Compounds $[Fe_3(CO)_{12}]$ [6], $[Ru_3(CO)_{12}]$ [7], and $[Os_3(CO)_{12}]$ [8]; were synthesized according to the published procedures.

2.2. Synthesis of C_6F_5S-$P(C_6H_5)_2$ (1)

A solution of toluene (50 mL), HSC_6F_5 (1.0 g, 0.66 mL, 4.99 mmol) and NEt_3 (50 mg, 0.70 mL, 4.99 mmol) was stirred under N_2 for 20 min. After this time a $(C_6H_5)_2PCl$ (1.102 g, 0.89 mL, 4.99 mmol) and toluene (20 mL) were added. Immediate formation of a white precipitated was noted. The mixture was stirred overnight, filtered and concentrated under reduced pressure. A microcrystalline white solid was obtained (92%). ^{1}H NMR (300 MHz, $CDCl_3$): δ 7.65 (m, 4H, H_o), 7.43 (m, 6H, $H_{m,p}$). $^{13}C\{^1H\}$NMR (75.5 MHz, $CDCl_3$): δ 149.70–146.43(C_o-F), 143.26–139.29(C_p-F), 139.71–135.99 (C_m-F), 132.95(C_o-H), 132.66(C_o-H), 129.96(C_p-H), 128.86(C_m-H), 128.78(C_m-H). $^{19}F\{^1H\}$NMR (282 MHz, $CDCl_3$): δ −128.96 (m, $^3J_{F_o-F_m} = 16.92$ Hz, F_o), −151.06 (t, $^3J_{F_p-F_m} = 22.56$ Hz, F_p), −159.36 (m, $^3J_{F_p-F_m,F_o-F_m} = 22.56, 16.92$ Hz, F_m). $^{31}P\{^1H\}$NMR (121 MHz, $CDCl_3$): δ 45.29 (t, $^4J = 18.16$ Hz). EI-MS: 385 (M^+, 89%), Anal. Calc. for $C_{18}H_{10}F_5PS$; C, 56.26; H, 2.62. Found C, 56.22; H, 2.59.

2.3. General procedure for the preparation of SP-transition metal clusters complexes

Complexes **2**–**4** were obtained using identical experimental procedures. As a representative example, the synthesis of $[Fe_2(\mu\text{-}SC_6F_5)(\mu\text{-}PPh_2)(CO)_6]$ (**2**) is described.

2.3.1. Synthesis of $[Fe_2(\mu\text{-}SC_6F_5)(\mu\text{-}PPh_2)(CO)_6]$ (2)

A mixture of the metal carbonyl complex $[Fe_3(CO)_{12}]$ (21.85 mg, 4.34 mmol), $(C_6F_5)S\text{-}P(C_6H_5)_2$ (50 mg, 13.02 mmol) and heptane (25 mL) was refluxed for 4 h. The solvent was removed under vacuum, the residue redissolved in a minimal volume of CH_2Cl_2, and filtered through a short plug of Celite®. Red crystals were grown by recrystallization from a heptane/dichloromethane (2:8) mixture. A microcrystalline red solid was obtained (94%); m.p. 186–187 °C. IR ($CHCl_3$): ν_{CO} 2070.98(m), 2031.82(s), 2004.09(vs), 1981.69(vs) cm^{-1}. ^{1}H NMR (300 MHz, $CDCl_3$): δ 7.60(t, 4 H, H_o), 7.37(s, 2H, H_p), 7.29 (2, 4H, H_m); $^{13}C\{^1H\}$NMR (75.5 MHz, $CDCl_3$): δ 207.94 (CO), 147.37–144.05 (C_o-F), 142.13–138.75 (C_p-F), 139.53–136.50 (C_m-F), 136.24–135.71 (C_{ipso}-P), 134.40 (d, $^3J = 8.15$ Hz, C_o-H), 133.33 (d, $^3J = 8.60$ Hz, C_o-H), 131.75-131.37 (C_{ipso}-S), 130.58 (d, C_p-H), 130.30(d, C_p-H), 128.75 (d, $^3J = 10.64$ Hz, C_m-H), 128.26 (d, $^3J = 10.17$ Hz, C_m-H); $^{19}F\{^1H\}$-NMR (282 MHz, $CDCl_3$): δ −124.13 (d, $^3J_{F_o-F_m} = 16.92$ Hz, F_o), −151.94 (t, $^3J_{F_p-F_m} = 19.74$ Hz, F_p), −159.79(m, $^3J_{F_p-F_m,F_o-F_m} = 19.74$, 16.92 Hz, F_m); $^{31}P\{^1H\}$NMR (121 MHz, $CDCl_3$): δ 138.66. FAB^+-MS $M^+ = 664$ *m/z*. Anal. Calc. for $C_{24}H_{10}F_5Fe_2O_6PS$ (664.05): C, 43.41; H, 1.52. Found: C, 43.38, H, 1.55.

2.3.2. Synthesis of $[Ru_4(\mu_3\text{-}SPPh_2)_2(\mu\text{-}SC_6F_5)_2(\mu\text{-}PPh_2)_2(SC_6F_5)_2(CO)_6]$ (3)

A red solid was obtained in 70% yield; m.p. 234–236 °C. IR ($CHCl_3$): ν_{CO} 2045(vs), 1979(vs) cm^{-1}. ^{1}H NMR (300 MHz, $CDCl_3$): δ 7.94–7.47(m, 40 H); ^{13}C NMR (75.5 MHz, $CDCl_3$): δ 133.65, 132.43, 131.56, 130.52, 129.783, 128.89, 128.26; $^{19}F\{^1H\}$NMR (282 MHz, $CDCl_3$): δ −124.92 and 128.92 (m, $^3J_{F_o-F_m} = 16.92$, F_o), −144.43 and −146.73 (m, $^3J_{F_p-F_m} = 22.56$, F_p), −154.74 and −158.36 (m, $^3J_{F_p-F_m,F_o-F_m} = 22.56$, 16.92 Hz, F*m*); $^{31}P\{^1H\}$NMR (121 MHz, $CDCl_3$) δ 106 (s), 145(s). FAB^+-MS $M^+ = 2174$ *m/z*. Anal. Calc. for $C_{78}H_{40}F_{20}Ru_4O_6P_4S_6$ (2173.62): C, 43.10; H, 1.85. Found: C, 43.08; H, 1.86.

2.3.3. Synthesis of $[Os_3(\eta^1\text{-}Ph_2P\text{-}SC_6F_5)(CO)_{11}]$ (4)

A microcrystalline pale yellow solid was obtained in 65% yield. Single crystal for X-ray diffraction study

was obtained from heptane–dichloromethane at room temperature; m.p. 218–220 °C. IR ($CHCl_3$): νCO 2068(m), 2027(vs), 1949(vs) cm^{-1}. ^1H NMR (300 MHz, $CDCl_3$) δ 7.59–7.44 (m, 10H); ^{13}C NMR (75.5 MHz, $CDCl_3$) δ 186.38 (CO), 134.22–133.31 (Co-F), 134.01–133.40 (C$_p$-F), 133.10 (C$_m$-F), 132.40 (d, $^3J_{C\text{-}P}$ = 12.45 Hz, C$_o$-H), 132.19 (s, C$_p$-H) 131.55 (d, $^3J_{C\text{-}P}$ = 12.19 Hz, C$_{ipso}$-P), 130.37 (d, $^3J_{C\text{-}P}$ = 12.19 Hz, C$_{ipso}$-S),128.78 (d, $^3J_{C\text{-}P}$ = 11.40 Hz, C$_m$-H); $^{19}F\{^1H\}$NMR (282 MHz, $CDCl_3$) δ-127.12 (d, $^3J_{F_o\text{–}F_m}$ = 19.74 Hz, F$_o$), −148.20 (t, $^3J_{F_p\text{–}F_m}$ = 19.74 Hz, F$_p$), −159.30 (m, $^3J_{F_p\text{–}F_m}$ = 19.74 Hz, F$_m$); $^{31}P\{^1H\}$NMR (121 MHz, $CDCl_3$) δ 70.35. FAB$^+$-MS M$^+$ = 1263. Anal. Calc. for $C_{29}H_{10}F_5O_{11}Os_3PS$ (1263.1): C, 27.58; H, 0.80. Found: C, 27.55; H, 0.79.

2.4. Data collection and refinement for [$Fe_2(\mu$-$SC_6F_5)$-$(\mu$-$PPh_2)(CO)_6$] (2), [$Ru_4(\mu_3$-$SPPh_2)_2(\mu$-$SC_6F_5)_2$-$(\mu$-$PPh_2)_2(SC_6F_5)_2(CO)_6$] (3), [$Os_3(\eta^1$-$Ph_2P$-$SC_6F_5)$-$(CO)_{11}$] (4)

Crystalline red, red-orange and yellow prisms for **2**, **3** and **4**, respectively, were grown independently by slow diffusion of CH_2Cl_2/heptane solvent systems. Each crystal was mounted on a glass fiber. In all cases, the X-ray intensity data were measured at 293 or 291 K on a Bruker SMART APEX CCD-based X-ray diffractometer system equipped with a Mo-target X-ray tube (λ = 0.71073 Å). The detector was placed at a distance of 4.837 cm from the crystals in all cases. A total of 1800 frames were collected with a scan width of 0.3° in ω and an exposure time of 10 s/frame. The frames were integrated with the Bruker SAINT software package [9] using a narrow-frame integration algorithm. The integration of the data was done using a triclinic unit cell in all cases except for complex **2** were a monoclinic unit cell was used to yield a total of 20030, 42663 and 32023 reflections for **2**, **3** and **4**, respectively, to a maximum 2θ angle of 50.00° (0.93 Å resolution), of which 4409 (**2**), 14466 (**3**) and 11567(**4**) were independent. Analysis of the data showed in all cases negligible decays during data collections. The structures were solved by Patterson method using SHELXS-97 [10] program. The remaining atoms were located via a few cycles of least squares refinements and difference Fourier maps, using the space group $P2_1/c$ with Z = 4 for **2**, $P\bar{1}$ with Z = 1 for **3** and $P\bar{1}$ with Z = 2 for **4**. Hydrogen atoms were input at calculated positions, and allowed to ride on the atoms to which they are attached. Thermal parameters were refined for hydrogen atoms on the phenyl groups using a U_{eq} = 1.2 Å to precedent atom in all cases. For all complexes, the final cycle of refinement was carried out on all non-zero data using SHELXL-97 [10] and anisotropic thermal parameters for all non-hydrogen atoms. The details of the structure determinations are given in Table 1 and selected bond lengths (Å) and angles (°) are given in Tables 2–4, respectively. The numbering of the atoms is shown in Figs. 1–3, respectively (ORTEP) [11].

Table 1
Summary of crystal structure data for: [$Fe_2(\mu$-$SC_6F_5)(\mu$-$PPh_2)(CO)_6$] (**2**), [$Ru_4(\mu_3$-$SPPh_2)_2(\mu$-$SC_6F_5)_2(\mu$-$PPh_2)_2(SC_6F_5)_2(CO)_6$] (**3**), [$Os_3(\eta^1$-$Ph_2P$-$SC_6F_5)(CO)_{11}$] (**4**)

Compound	**2**	**3**	**4**
Formula	$C_{24}H_{10}F_5Fe_2O_6PS$	$C_{78}H_{40}F_{20}Ru_4O_6P_4S_6$	$C_{29}H_{10}F_5O_{11}Os_3PS$
Formula weight	664.05	2173.62	1263.00
Crystal system	Monoclinic	Triclinic	Triclinic
Space group	$P2_1/c$	$P\bar{1}$	$P\bar{1}$
a (Å)	14.5431(9)	12.524(3)	8.1154(4)
b (Å)	10.8230(6)	14.753(4)	13.4111(7)
c (Å)	15.9483(9)	16.075(4)	16.5814(9)
α (°)	90	90	108.80(1)
β (°)	93.3170(10)	112.18(1)	90.718(1)
γ (°)	90	90	106.581(1)
V (Å^3)	2506.1(3)	2470.4(11)	1626.4(2)
Z	4	1	2
ρ_{calc} (g cm^{-3})	1.760	1.461	2.579
μ (mm^{-1})	1.320	0.872	11.891
Reflections collected	20,030	42,663	32,023
Independent reflections	4409 [R_{int} = 0.0377]	14466 [R_{int} = 0.0942]	11567 [R_{int} = 0.0651]
GOF on F^2	1.008[a]	1.011[a]	1.002[a]
$R(I>2\sigma(I))$	R_1 = 0.0360, wR_2 = 0.0758[a]	R_1 = 0.0683, wR_2 = 0.2017[a]	R_1 = 0.0429, wR_2 = 0.0704[a]
R indices (all data)	$R1$ = 0.0440, wR_2 = 0.0791[b]	R_1 = 0.02122, wR_2 = 0.02270[b]	R_1 = 0.0730, wR_2 = 0.0931[b]

[a] $S = [(w(F_o)^2 - (F_c)^2)^2/(n-p)]^{1/2}$, where n = number of reflections and p = total number of parameters.
[b] $R_1 = |F_o - F_c|/|F_o|$, $wR_2 = [w((F_o)^2 - (F_c)^2)^2/w(F_o)^2]^{1/2}$.

Table 2
Selected bond lengths and angles for $[Fe_2(\mu\text{-}SC_6F_5)(\mu\text{-}PPh_2)(CO)_6]$ (**2**)

Bond lengths (Å)		Angles (°)	
Fe(1)–C(3)	1.780(3)	C(3)–Fe(1)–C(2)	100.34(13)
Fe(1)–C(2)	1.792(3)	C(3)–Fe(1)–C(1)	88.83(12)
Fe(1)–C(1)	1.814(3)	C(2)–Fe(1)–C(1)	100.63(12)
Fe(1)–P(1)	2.2281(8)	C(3)–Fe(1)–P(1)	90.95(9)
Fe(1)–S(1)	2.2781(7)	C(2)–Fe(1)–P(1)	100.85(9)
Fe(1)–Fe(2)	2.5394(5)	C(1)–Fe(1)–P(1)	158.20(9)
Fe(2)–C(4)	1.786(3)	C(3)–Fe(1)–S(1)	153.13(9)
Fe(1)–C(5)	1.792(3)	C(2)–Fe(1)–S(1)	105.06(9)
Fe(2)–C(6)	1.809(3)	C(1)–Fe(1)–S(1)	94.89(9)
Fe(2)–P(1)	2.2298(8)	P(1)–Fe(1)–S(1)	75.94(3)
Fe(2)–S(1)	2.2853(7)	C(3)–Fe(1)–Fe(2)	96.91(9)
O(1)–C(1)	1.127(3)	C(2)–Fe(1)–Fe(2)	150.82(9)
O(2)–C(2)	1.133(3)	C(1)–Fe(1)–Fe(2)	103.09(8)
O(3)–C(3)	1.135(3)	P(1)–Fe(1)–Fe(2)	55.30(2)
O(4)–C(4)	1.130(3)	S(1)–Fe(1)–Fe(2)	56.32(2)
O(5)–C(6)	1.129(3)	C(4)–Fe(2)–C(5)	98.16(13)
O(6)–C(5)	1.135(3)	C(4)–Fe(2)–C(6)	91.05(12)
		C(5)–Fe(2)–C(6)	99.42(13)
		C(4)–Fe(2)–P(1)	94.84(9)
		C(5)–Fe(2)–P(1)	107.10(10)
		C(6)–Fe(2)–P(1)	152.85(9)
		C(4)–Fe(2)–S(1)	156.75(9)
		C(5)–Fe(2)–S(1)	103.88(10)
		C(6)–Fe(2)–S(1)	92.57(9)
		P(1)–Fe(2)–S(1)	75.76(3)
		C(4)–Fe(2)–Fe(1)	100.70(9)
		C(5)–Fe(2)–Fe(1)	154.08(10)
		C(6)–Fe(2)–Fe(1)	97.85(9)
		P(1)–Fe(2)–Fe(1)	55.24(2)
		S(1)–Fe(2)–Fe(1)	56.05(2)
		C(7)–S(1)–Fe(1)	117.30(9)
		C(7)–S(1)–Fe(2)	114.54(9)
		Fe(1)–S(1)–Fe(2)	67.62(2)
		Fe(1)–P(1)–Fe(2)	69.45(2)
		O(1)–C(1)–Fe(1)	177.7(3)
		O(2)–C(2)–Fe(1)	177.5(3)
		O(3)–C(3)–Fe(1)	177.0(3)
		O(4)–C(4)–Fe(2)	178.2(3)
		O(6)–C(5)–Fe(2)	177.7(3)
		O(5)–C(6)–Fe(2)	179.0(3)

Table 3
Selected bond lengths and angles for $[Ru_4(\mu_3\text{-}SPPh_2)_2(\mu\text{-}SC_6F_5)_2(\mu\text{-}PPh_2)_2(SC_6F_5)_2(CO)_6]$ (**3**)

Bond lengths (Å)		Angles (°)	
Ru(1)–C(38)	1.888(11)	C(38)–Ru(1)–C(39)	89.1(4)
Ru(1)–C(39)	1.912(11)	C(38)–Ru(1)–P(1)	94.0(3)
Ru(1)–P(1)	2.357(3)	C(39)–Ru(1)–P(1)	95.5(3)
Ru(1)–S(1)	2.465(3)	C(38)–Ru(1)–S(1)	94.9(3)
Ru(1)–S(2)	2.494(3)	C(39)–Ru(1)–S(1)	176.0(3)
Ru(1)–S(2)#1	2.522(3)	P(1)–Ru(1)–S(1)	83.82(10)
Ru(2)–C(37)	1.877(10)	C(38)–Ru(1)–S(2)	176.2(3)
Ru(2)–P(2)	2.275(3)	C(39)–Ru(1)–S(2)	94.6(3)
Ru(2)–P(1)	2.307(3)	P(1)–Ru(1)–S(2)	86.49(9)
Ru(2)–S(3)	2.335(3)	S(1)–Ru(1)–S(2)	81.43(9)
Ru(2)–S(1)	2.449(3)	C(38)–Ru(1)–S(2)#1	96.1(3)
S(1)–C(1)	1.739(11)	C(39)–Ru(1)–S(2)#1	100.3(3)
S(2)–P(2)	2.125(4)	P(1)–Ru(1)–S(2)#1	161.29(10)
S(2)–Ru(1)#1	2.522(3)	S(1)–Ru(1)–S(2)#1	79.68(9)
S(3)–C(7)	1.759(14)	S(2)–Ru(1)–S(2)#1	82.40(8)
O(1)–C(37)	1.123(11)	C(37)–Ru(2)–P(2)	95.1(3)
O(2)–C(38)	1.120(10)	C(37)–Ru(2)–P(1)	94.5(3)
O(3)–C(39)	1.125(11)	P(2)–Ru(2)–P(1)	86.35(10)
		C(37)–Ru(2)–S(3)	93.9(3)
		P(2)–Ru(2)–S(3)	139.55(12)
		P(1)–Ru(2)–S(3)	132.07(12)
		C(37)–Ru(2)–S(1)	177.1(3)
		P(2)–Ru(2)–S(1)	82.04(9)
		P(1)–Ru(2)–S(1)	85.25(9)
		S(3)–Ru(2)–S(1)	88.41(10)
		Ru(2)–S(1)–Ru(1)	90.73(9)
		P(2)–S(2)–Ru(1)	101.13(13)
		P(2)–S(2)–Ru(1)#1	123.43(13)
		Ru(1)–S(2)–Ru(1)#1	97.60(8)
		Ru(2)–P(1)–Ru(1)	97.14(10)
		S(2)–P(2)–Ru(2)	112.56(13)
		O(1)–C(37)–Ru(2)	177.4(10)
		O(2)–C(38)–Ru(1)	177.8(10)
		O(3)–C(39)–Ru(1)	174.2(10)

3. Results and discussion

The thiophosphinite $C_6F_5S\text{-}P(C_6H_5)_2$ (**1**) has been conveniently synthesized from the reaction of stoichiometric amounts of pentafluorothiophenol (HSC_6F_5) and diphenylchlorophosphine (PPh_2PCl) in the presence of triethylamine (NEt_3) as base. This compound was obtained as a microcrystalline white solid. Analysis by ^1H NMR reveal the presence of the aromatic groups at 7.20–7.50 ppm. The analysis by $^{31}P\{^1H\}$NMR spectra were more informative, showing a unique signal at 45.29 ppm as a triplet, the multiplicity being the result of the P–F coupling ($^4J = 18.2$ Hz). The $^{19}F\{^1H\}$NMR spectrum of this compound reveal the fluorinated thiolates to be present, with typical splitting patterns for the ligand $^-SC_6F_5$. Thus a multiplet centered at −128.96 ppm is observed for the fluorines in the *ortho* position, a triplet centered at −151.06 ppm, corresponding to the fluorine in the *para* position and a multiplet at −159.36 ppm due to the presence of the fluorines in the *meta* position.

The reactivity of this compound was explored with transition metal carbonyl clusters. Thus, the reaction of three equivalents of compound **1** with one equivalent of $[Fe_3(CO)_{12}]$ under reflux conditions in heptane, affords complex $[Fe_2(\mu\text{-}SC_6F_5)(\mu\text{-}PPh_2)(CO)_6]$ (**2**) in good yield. This compound resulted from cleavage of the S–P bond. The infrared analysis for this compound reveals signals corresponding to the presence of the carbonyls between 1981 and 2070 cm^{-1}. Analysis of this complex by ^1H NMR shows signals in the usual region for aromatic protons. The ^{31}P NMR spectrum of this complex is more informative exhibiting a singlet at 138.66 ppm that accounts for a single phosphorus in the molecule, the chemical shift observed agrees well with the presence of a bridging phosphide ligand. The $^{19}F\{^1H\}$NMR spectra for this complex indicates the presence of the thiolate

Table 4
Selected bond lengths and angles for $[Os_3(\eta^1\text{-}Ph_2P\text{-}SC_6F_5)(CO)_{11}]$ (**4**)

Bond lengths (Å)		Angles (°)	
Os(1)–C(1)	1.893(7)	C(1)–Os(1)–C(2)	91.8(3)
Os(1)–C(2)	1.939(7)	C(1)–Os(1)–C(3)	90.0(3)
Os(1)–C(3)	1.942(7)	C(2)–Os(1)–C(3)	178.2(3)
Os(1)–P(1)	2.3179(18)	C(1)–Os(1)–P(1)	100.1(2)
Os(1)–Os(2)	2.8831(4)	C(2)–Os(1)–P(1)	87.8(2)
Os(1)–Os(3)	2.9008(4)	C(3)–Os(1)–P(1)	91.8(2)
Os(2)–C(4)	1.882(9)	C(1)–Os(1)–Os(2)	97.2(2)
Os(2)–C(5)	1.922(8)	C(2)–Os(1)–Os(2)	84.5(2)
Os(2)–C(7)	1.941(7)	C(3)–Os(1)–Os(2)	95.3(2)
Os(2)–C(6)	1.942(8)	P(1)–Os(1)–Os(2)	161.32(4)
Os(2)–Os(3)	2.8846(4)	C(1)–Os(1)–Os(3)	156.2(2)
Os(3)–C(8)	1.918(8)	C(2)–Os(1)–Os(3)	92.01(19)
Os(3)–C(9)	1.919(8)	C(3)–Os(1)–Os(3)	86.4(2)
Os(3)–C(11)	1.950(8)	P(1)–Os(1)–Os(3)	103.58(4)
Os(3)–C(10)	1.954(8)	Os(2)–Os(1)–Os(3)	59.831(10)
P(1)–S(1)	2.142(2)	C(4)–Os(2)–C(5)	101.9(4)
O(1)–C(1)	1.137(7)	C(4)–Os(2)–C(7)	91.2(3)
O(2)–C(2)	1.135(8)	C(5)–Os(2)–C(7)	91.6(3)
O(3)–C(3)	1.133(8)	C(4)–Os(2)–C(6)	90.1(3)
O(4)–C(4)	1.147(9)	C(5)–Os(2)–C(6)	89.4(3)
O(5)–C(5)	1.127(8)	C(7)–Os(2)–C(6)	178.2(3)
O(6)–C(6)	1.140(9)	C(4)–Os(2)–Os(1)	160.1(3)
O(7)–C(7)	1.135(8)	C(5)–Os(2)–Os(1)	97.7(2)
O(8)–C(8)	1.128(9)	C(7)–Os(2)–Os(1)	84.7(2)
O(9)–C(9)	1.128(9)	C(6)–Os(2)–Os(1)	93.7(2)
O(10)–C(10)	1.130(8)	C(4)–Os(2)–Os(3)	100.3(3)
O(11)–C(11)	1.128(8)	C(5)–Os(2)–Os(3)	157.5(2)
		C(7)–Os(2)–Os(3)	91.2(2)
		C(6)–Os(2)–Os(3)	87.3(2)
		Os(1)–Os(2)–Os(3)	60.390(9)
		C(8)–Os(3)–C(9)	101.0(3)
		C(8)–Os(3)–C(11)	91.0(3)
		C(9)–Os(3)–C(11)	90.3(3)
		C(8)–Os(3)–C(10)	91.2(3)
		C(9)–Os(3)–C(10)	91.1(3)
		C(11)–Os(3)–C(10)	177.1(3)
		C(8)–Os(3)–Os(2)	98.6(2)
		C(9)–Os(3)–Os(2)	160.2(2)
		C(11)–Os(3)–Os(2)	86.7(2)
		C(10)–Os(3)–Os(2)	91.1(2)
		C(8)–Os(3)–Os(1)	158.0(2)
		C(9)–Os(3)–Os(1)	100.8(2)
		C(11)–Os(3)–Os(1)	91.6(2)
		C(10)–Os(3)–Os(1)	85.59(19)
		Os(2)–Os(3)–Os(1)	59.779(9)
		C(18)–P(1)–C(12)	101.6(3)
		C(18)–P(1)–S(1)	107.2(2)
		C(12)–P(1)–S(1)	103.0(2)
		C(18)–P(1)–Os(1)	118.5(2)
		C(12)–P(1)–Os(1)	118.8(2)
		S(1)–P(1)–Os(1)	106.35(9)
		C(24)–S(1)–P(1)	107.6(2)

moiety in the molecule with signals at −124.13 (F_o), −151.94 (F_p) and −159.79 (F_m) ppm with typical splitting patterns for the ligand $^{-}SC_6F_5$. Further analysis of this complex by LSIMS exhibits the molecular ion for the complex $[M^+] = 664$ *m*/*z*.

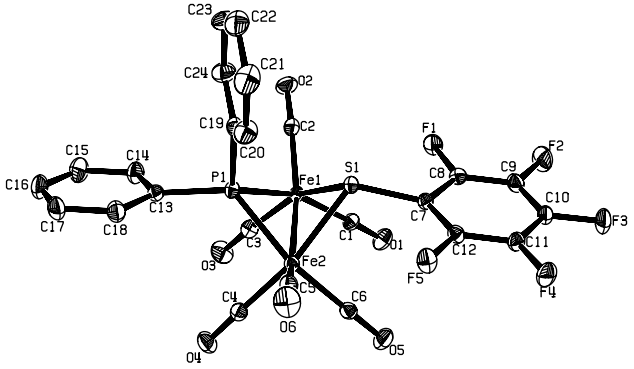

Fig. 1. An ORTEP representation of the structure of $[Fe_2(\mu\text{-}SC_6F_5)(\mu\text{-}PPh_2)(CO)_6]$ (**2**) at 50% probability showing the atom labeling scheme.

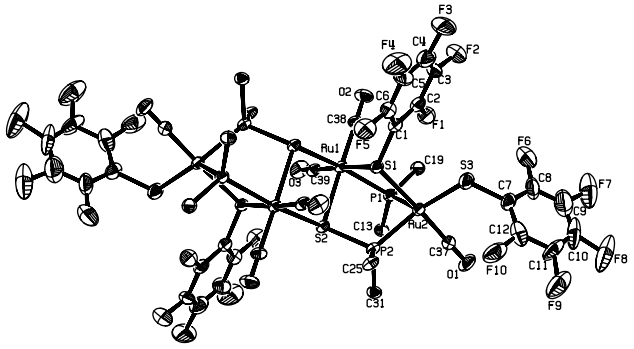

Fig. 2. An ORTEP representation of the structure of $[Ru_4(\mu_3\text{-}SPPh_2)_2(\mu\text{-}SC_6F_5)_2(\mu\text{-}PPh_2)_2(SC_6F_5)_2(CO)_6]$ (**3**) at 50% probability showing the atom labeling scheme.

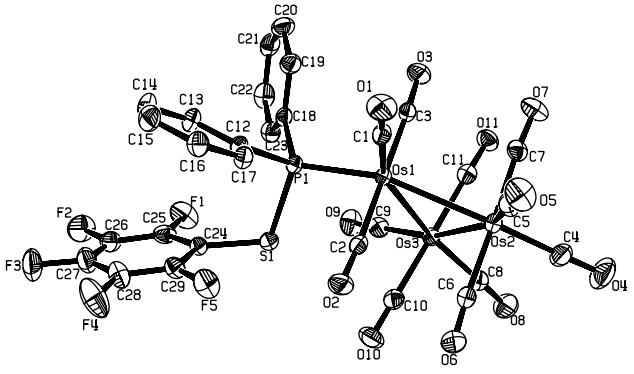

Fig. 3. An ORTEP representation of the structure of $[Os_3(\eta^1\text{-}Ph_2P\text{-}SC_6F_5)(CO)_{11}]$ (**4**) at 50% probability showing the atom labeling scheme.

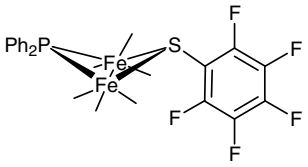

Crystals suitable for X-ray diffraction analysis of complex **2** were obtained from a heptane/dichloromethane solvent system. Analysis of the red crystals revealed a dinuclear structure bridged by $^{-}PPh_2$ and $^{-}SC_6F_5$ moieties generating a butterfly like structure, which resulted from P–S bond cleavage of compound **1** (Fig. 1). The two iron centers have a distorted geometry octahedral. The coordination sphere is completed by six terminal carbonyl ligands, three for each iron fragment. In all other respects the bond distances and angles are within the expected values (Table 2).

Ruthenium compounds and particularly, $[Ru_3(CO)_{12}]$ has been recognized and used as a model for HDS processes in homogeneous catalysis [12]. Thus it is not surprising that the reaction of C_6F_5S-$P(C_6H_5)_2$ (**1**) with $[Ru_3(CO)_{12}]$ affords a product that goes beyond the mere activation of the P–S bond, affording complex $[Ru_4(\mu_3\text{-}SPPh_2)_2(\mu\text{-}SC_6F_5)_2(\mu\text{-}PPh_2)_2(SC_6F_5)_2(CO)_6]$ (**3**), which is the result of the P–S bond cleavage and the activation of the C–S bond of the fluorinated thiolate moiety. As a result of the presence of sulfur in the molecule the structure is more complicated than expected. Infrared analysis reveals absorptions due to the presence of the carbonyl ligands between 1979 and 2045 cm^{-1}. The presence of the aromatic protons were detected in the region 7.94–7.47 ppm. The $^{31}P\{^1H\}$NMR spectrum is more instructive since it shows signals at 145 and 106 ppm. The signal at 145 ppm is due to the phosphorus moiety bridging the two ruthenium centers and the other bridges between one ruthenium center and one sulfur (vide infra). The analysis by ^{19}F NMR exhibits signals with typical splitting patterns for $^{-}SC_6F_5$, the sets of signals are duplicated (δ −124.92 (d) and −128.92 (t) F_o, −144.43 (d) and −146.73 (t) F_p, −154.74 (d) and −158.36 (t) F_m) due to the presence of two different types of thiolates, one bridging and one terminal. FAB^+-MS analysis identified the molecular ion $[M^+] = 2174$ *m*/*z*.

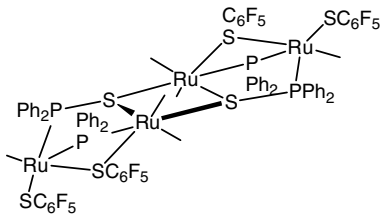

In order to know the faith of the C_6F_5 group lost from the thiolate moiety, some of the mother liquor from the reaction mixture was taken and analyzed by GC–MS, the results reveal the presence of $P(C_6F_5)(C_6H_5)_2$ in the solution, this compound is indeed the result of the C–S activation process and probably also consequence of a partial decomposition of the ligand C_6F_5S-$P(C_6H_5)_2$ (**1**) during the reaction.

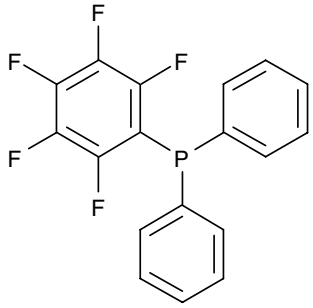

Slow diffusion of heptane into a saturated solution of $[Ru_4(\mu_3\text{-}SPPh_2)_2(\mu\text{-}SC_6F_5)_2(\mu\text{-}PPh_2)_2(SC_6F_5)_2(CO)_6]$ (**3**) in CH_2Cl_2 at room temperature, afforded red-orange crystals. X-ray diffraction analysis revealed a tetrameric structure consisting of two different ruthenium centers. One is in a distorted trigonal bipyramidal (TBP) environment, and the other having a slightly distorted octahedral geometry bridged by μ_3-$SPPh_2$, μ-SC_6F_5 and μ-PPh_2 moieties. The coordination spheres are completed by one terminal $^{-}SC_6F_5$ and one carbonyl ligand for the TBP center, while the octahedron is completed by two terminal carbonyl ligands and the sulfur of another μ_3-$SPPh_2$ moiety. The bond distances and angles are comparable to those found in complexes such as $[Ru_3(\mu\text{-}Se)(\mu\text{-}PPh_2)(\mu\text{-pyth})(CO)_6\{P(pyth)Ph_2\}]$-pyth = 5-(2-pyridyl)-2-thienyl [13]. $[Ru_3(CO)_6(\mu_3\text{-}CO)(\mu_3\text{-}Se)(\mu\text{-dppm})(\eta^1\text{-}Ph_2PCH_2P(=O)Ph_2)]$ [14] and $[Ru_3(\mu\text{-}H)\{\mu\text{-}P(C_4H_2S)Ph_2\}(CO)_8\{P(C_4H_3S)Ph_2\}]$ [15]. In all other respects the bond distances and angles are within the expected values (Table 3).

Finally, the reaction of C_6F_5S-$P(C_6H_5)_2$ (**1**) with $[Os_3(CO)_{12}]$ seems to be the milder of all three processes, since under reflux in heptane it afforded $[Os_3(\eta^1\text{-}PPh_2\text{-}SC_6F_5)(CO)_{11}]$ (**4**) as the sole product. Complex 4 resulted from *P*-coordination to one of the osmium centers of the cluster.

Infrared analysis of this complex reveals the presence of the carbonyl ligands exhibiting absorptions between 1949 and 2068 cm^{-1}. As in the previous case, ^1H NMR of this complex exhibits signals corresponding to the presence of the protons on the phenyl moiety at 7.59–7.44 ppm. Similarly, analysis by ^{19}F NMR exhibits signals at −127.12 (F_o), −148.20 (F_p) and −159.30 (F_m) ppm with the typical splitting patterns for the ligand $^{-}SC_6F_5$. Analysis by FAB^+-MS as in the previous cases exhibits the molecular ion for complex **3**, $[M^+] = 1263$ *m*/*z*.

In all cases, elemental analysis for the complexes agreed with the proposed formulations.

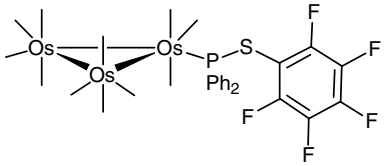

Recrystalization of complex **4** from a CH_2Cl_2/heptane solvent system afford pale yellow crystals. Analysis of this compound by single crystal X-ray diffraction analysis, revealed a compound where the starting material $[Os_3(CO)_{12}]$ had lost one carbonyl, which was substituted by the compound $C_6F_5S\text{-}P(C_6H_5)_2$ (**1**). In this case, the structure of the P–S ligand remains intact after the reaction. The bond distances and angles are similar to those observed for the starting material $[Os_3(CO)_{12}]$ [16]. The P(1)–S(1) distance 2.142 Å is considerably larger than that found in $[Co_2(\mu\text{-}HCCH)(CO)_4\{PPh_2(S\text{-}Bu^n)\}_2]$ [17]. Unfortunately, no direct comparison can be done with the free ligand $C_6F_5S\text{-}P(C_6H_5)_2$ (**1**), since several attempts to attain suitable crystals afforded agglomerated crystals.

It is well known that complexes of the transition metals become progressively more inert as the periodic group is descended. Thus, in conclusion, we can say that the reactivity observed clearly illustrates, in the first instance the degree of robustness of the M–M bonds and that the reactivity seems to be ruled by the nature of the metal in each case. In addition, the osmium compound $[Os_3(\eta^1\text{-}PPh_2\text{-}SC_6F_5)(CO)_{11}]$ (**4**) seems to be an ideal candidate to further explore its reactivity, and it can be envisaged as a model intermediate for the reactions leading to complexes **2** and **3**. Efforts aimed at exploring this possibility are currently under way. Moreover, we have shown that the ligand $C_6F_5S\text{-}P(C_6H_5)_2$ (**1**) can indeed serve as convenient source of phosphido and thiolate ligands, and given the observed coordination versatility of this ligand it would be important to explore its reactivity with other transition metal starting materials.

Acknowledgements

O.B.-P. and G.R.-M. thank CONACYT for financial support. We thank Chem. Eng. Luis Velasco Ibarra, M. Sc. Francisco Javier Pérez Flores, QFB. Ma del Rocío Pati simno and Ma. de las Nieves Zavala for their invaluable help in the running of the FAB^+-Mass, IR and $^{19}F\{^1H\}$ spectra, respectively. We thank Prof. T.K. Hollis for helpful suggestions and careful proof reading of the manuscript. The support of this research by CONACYT (J41206-Q) is gratefully acknowledged.

Appendix A. Supplementary material

Supplementary data for complexes **2**, **3** and **4** have been deposited at the Cambridge Crystallographic Data Centre. Copies of this information are available free of charge on request from The Director, CCDC, 12 Union Road, Cambridge, CB2 1EZ, UK (fax: +44 1223 336033; e-mail deposit@ccdc.cam.ac.uk or www: http://www.ccdc.cam.ac.uk) quoting the deposition numbers CCDC 257187 trough 257189. Supplementary data associated with this article can be found, in the online version at doi:10.1016/j.jorganchem.2005.02.046.

References

[1] M.L. Steigerwald, Polyhedron 13 (1994) 1245.
[2] (a) For reviews on the use of molecular compounds as models for HDS process see: R.J. Angelici, Acc. Chem. Res. 21 (1988) 387;
(b) R.J. Angelici, Coord. Chem. Rev. 105 (1990) 61;
(c) T.B. Rauchfuss, Prog. Inog. Chem. 39 (1991) 251;
(d) R. Sánchez-Delgado, J. Mol. Catal. 86 (1994) 287;
(e) C. Bianchini, A. Meli, J. Chem. Soc., Dalton. Trans. (1996) 801;
(f) R.J. Angelici, Polyhedron 16 (1997) 3073.
[3] H. Topsøe, B.S. Clausen, F.E. Massoth, in: J.R. Anderson, M. Boudart (Eds.), Hydrotreating Catalysis: Science and Technology, vol. 11, Springer-Verlag, Berlin, 1996.
[4] (a) D. Fenske, G. Longoni, G. Schmid, in: G. Schimid (Ed.), Clusters and Colloids, VCH, Weinheim, 1994 (Chapter 3);
(b) G. Henkel, Weissgraber, in: P. Braunstein, L. Oro, P. Raithby (Eds.), Metal Clusters in Chemistry, vol. 1, VCH, Weinheim, 1999.
[5] (a) D. Morales-Morales, R. Redón, Y. Zheng, J.R. Dilworth, Inorg. Chim. Acta 328 (2002) 39;
(b) D. Morales-Morales, C. Grause, K. Kasaoka, R. Redón, R.E. Cramer, C.M. Jensen, Inorg. Chim. Acta 300–302 (2000) 958;
(c) D. Morales-Morales, R. Redón, C. Yung, C.M. Jensen, Chem. Commun. (2000) 1619;
(d) D. Morales-Morales, R. Redón, Z. Wang, D.W. Lee, C. Yung, K. Magnuson, C.M. Jensen, Can. J. Chem. 79 (2001) 823;
(e) D. Morales-Morales, R.E. Cramer, C.M. Jensen, J. Organomet. Chem. 654 (2002) 44;
(f) X. Gu, W. Chen, D. Morales-Morales, C.M. Jensen, J. Mol. Catal. A 189 (2002) 119;
(g) J.R. Dilworth, P. Arnold, D. Morales, Y.L. Wong, Y. Zheng, The chemistry and applications of complexes with sulphur ligands, in: Modern Coordination ChemistryThe Legacy of Joseph Chatt, Royal Society of Chemistry, Cambridge, UK, 2002, p. 217;
(h) D. Morales-Morales, S. Rodríguez-Morales, J.R. Dilworth, A. Sousa-Pedrares, Y. Zheng, Inorg. Chim. Acta 332 (2002) 101;
(i) V. Gómez-Benítez, S. Hernández-Ortega, D. Morales-Morales, Inorg. Chim. Acta 346 (2003) 256;
(j) D.W. Lee, C.M. Jensen, D. Morales-Morales, Organometallics 22 (2003) 4744;
(k) V. Gómez-Benítez, S. Hernández-Ortega, D. Morales-Morales, J. Mol. Struct. 689 (2004) 137;
(l) D. Morales-Morales, R. Redón, C. Yung, C.M. Jensen, Inorg. Chim. Acta 357 (2004) 2953;
(m) C. Herrera-Álvarez, V. Gómez-Benítez, R. Redón, J.J. García, S. Hernández-Ortega, R.A. Toscano, D. Morales-Morales, J. Organomet. Chem. 689 (2004) 2464;
(n) G. Ríos-Moreno, R.A. Toscano, R. Redón, H. Nakano, Y. Okuyama, D. Morales-Morales, Inorg. Chim. Acta 358 (2005) 303.
[6] W. McFarlane, G. Wilkinson, Inorg. Synth. 8 (1966) 181.
[7] M.I. Bruce, C.M. Jensen, N.L. Jones, Inorg. Synth. 28 (1989) 216.

[8] S.R. Drake, P.A. Loveday, Inorg. Synth. 28 (1989) 230.
[9] Bruker AXS, SAINT Software Reference Manual, Madison, WI, 1998.
[10] G.M. Sheldrick, SHELXTL NT Version 6.10, Program for Solution and Refinement of Crystal Structures, University of Göttingen, Germany, 2000.
[11] L.J. Farrugia, ORTEP-3 for Windows, J. Appl. Crystallogr. 30 (1997) 565.
[12] A. Chehata, A. Oviedo, A. Arévalo, S. Bernès, J.J. García, Organometallics 22 (2003) 1585.
[13] D. Cauzzi, C. Graiff, Ch. Massera, G. Predieri, A. Tiripicchio, J. Cluster Sci. 12 (2001) 259.
[14] S.E. Kabir, S.J. Ahmed, Md.I. Hyder, Md.A. Miah, D.W. Bennet, D.T. Haworth, T.A. Siddiquee, E. Rosenberg, J. Organomet. Chem. 689 (2004) 3412.
[15] A.J. Deeming, S.N. Jayasuriya, A. Arce, Y. De Sanctis, Organometallics 15 (1996) 786.
[16] E.R. Corey, L.F. Dahl, Inorg. Chem. 1 (1962) 521.
[17] G. Conole, M. Kessler, M.J. Mays, G.E. Pateman, G.A. Solan, Polyhedron 17 (1998) 2993.